Rates and Mechanisms of Conversion of Ice Nanocrystals to Hydrates of HCl and HBr: Acid Diffusion in the Ionic Hydrates

J. Paul Devlin,*,† Dheeraj B. Gulluru,† and Victoria Buch‡

Department of Chemistry, Oklahoma State University, Stillwater, Oklahoma 74078, and The Fritz Haber Institute for Molecular Dynamics, The Hebrew University, Jerusalem, 91904, Israel

Received: September 26, 2004; In Final Form: November 17, 2004

This FTIR study focuses on solid-state chemistry associated with formation and interconversion of the ionic HX (X = Cl, Br) hydrates. Kinetic data are reported for conversions of ice nanocrystal arrays exposed to the saturation pressure of the acids in the 110∼125 K range. The product is amorphous acid dihydrate in the case of HBr, and amorphous monohydrate for HCl. The rate-determining step is identified as HX diffusion through the hydrate product crust toward the interfacial reaction zone, rather than diffusion through ice, as commonly believed. Slowing of the conversion process is thus observed with increasing thickness of the crust. The diffusion coefficient (D_e) and activation energy values for HX diffusion through the hydrates were evaluated with the help of the shrinking-core model. Hydrate crystallization occurs as a separate step, upon heating above 130 K. Subsequently, rates of reversible transitions between crystal di- and monohydrates were observed upon exposure to acid vapor and acid evacuation. In conversion from di- to monohydrate, the rate slows after fast formation of several layers; subsequently, diffusion through the product crust appears to be the rate-controlling step. The activation energy for HBr diffusion through crystal dihydrate is found to be significantly higher than that for the amorphous analogue. Conjecture is offered for a molecular mechanism of HX transport through the crystal hydrate, based on (i) spectroscopic/computational evidence for the presence of molecular HX bonded to X^- in each of the ionic hydrate phases and (ii) the relative E_a values found for HBr and HCl diffusion. Monte Carlo modeling suggests acid transport to the reaction zone along boundaries between "nanocrystallites" generated by multiple hydrate nucleation events at the particle surfaces. The reverse conversion, of crystalline monohydrate particles to the dihydrate phase, as well as dihydrate to trihydrate, displays nearly constant rate throughout the particle conversion; suggesting desorption of HX from the particle surface as the rate-limiting factor. Like for D_e, the activation energies for desorption were found to be ∼20% greater for HCl than HBr for related hydrate phases.

1. Introduction

Rate factors for the conversion of ice particles to a mixed-solid phase, through interactions with molecular adsorbates, have implications for science of the atmosphere, planets, and interstellar media. For this reason there have been an abundance of studies during the past decade designed to reveal the nature of the uptake and subsequent H-bond chemistry of strong adsorbates at the surface of ice films (for a recent review, see ref 1). Many of these studies have focused on characteristics of the uptake of vapors of strong acids such as HCl and HBr (HX).[2−8] Some were based on mass spectroscopic monitoring of acid vapors passed over ice films within a flow tube reactor[9,10] or on the time of residence of HX molecules from incident molecular beams.[4,7,8] Spectroscopic monitoring of the fate of the adsorbed gas on ice films has added a valuable dimension to these studies,[8,11−14] as have temperature-programmed[15−17] and laser desorption measurements.[6,18−20]

Results have often been related to diffusion of the acid species into ice.[9,21−24] However, in contrast to liquid H_2O, ice is a very poor solvent of isolated molecules. In particular, HCl solubility in ice was shown to be of the order of 1 ppm,[25] suggesting negligible contribution from motion of isolated acid molecules into ice crystals. (Motion along ice grain boundaries may still be efficient,[5] but would not lead to mixed-solid formation.) On the other hand, water molecules readily form compound solids with added molecular species. Thus hydrate formation can better be treated as a solid-phase reaction rather than as a result of dissolution of isolated molecules in ice.

This point of view is consistent with our recent FTIR investigations of the kinetics of mixed solid formation. Specifically, FTIR investigations have been carried out of the rates of conversion of ice nanocrystals within 3-D arrays to ammonia[26] and acid hydrate[27] particles. The well-established shrinking-core model of particle-adsorbate reaction[28,29] applies to these systems in the presence of an abundance of adsorbate (and, more generally, to the later stages of reaction of larger particles). This implies that the diffusion of the adsorbate through the product crust encasing a reacting particle core (a necessary aspect of any particle reaction mechanism) is the rate-controlling factor. Such diffusion moves the adsorbed reactant to the reaction zone at the interface of the ice core and the product crust. The corresponding HX diffusion rates within solid acid hydrates, which often govern the rate of the H-bond chemistry leading to a new phase,[26,27] have generally not been determined before from the ice-film studies. The diffusion coefficient (D_e) can be determined by applying the shrinking-core model to quantitative FTIR data and the activation energies

* Corresponding author. E-mail: devlin@okstate.edu.
† Oklahoma State University.
‡ The Hebrew University.

10.1021/jp0456281 CCC: $30.25
Published on Web 02/05/2005

of diffusion obtained from the temperature-dependent rates of reaction.[26,27] (Similar conclusions, regarding the role of diffusion through the product layer, have been reached in conversion studies of much larger ice particles to the clathrate hydrate of methane at much higher temperatures.[30])

The kinetic studies of the conversion of ice nanocrystals to particles of a hydrate (as well as the interconversion of particles of one hydrate with that of another)[31] have followed the development of methods to prepare 3-D arrays of nanocrystals of cubic ice.[32] Such arrays assemble naturally on surfaces within double-walled cold collisional-cooling cells in which ice aerosols are prepared. For example, 3-D arrays of ~20 nm average diameter ice crystals form when ~1% mixtures of water in helium are rapidly expanded into a cell held near 120 K. At this temperature, ~4% of the particles of an aerosol attach to the two ZnS windows of the inner cell chamber. The thickness of an array can be controlled by multiple loading and pump cycles so that samples are obtained of an optimum optical density for FTIR transmission spectroscopic measurements. The FTIR spectra allow ready identification and quantitation of the ice as well as the hydrates that form from reaction with the ice.

As in the aerosol phase from which they are formed, the distribution of particles with respect to size within a 3-D array is thought to follow a log-normal distribution.[33] Because of Ostwald ripening of the particles (i.e., growth of large particles by vapor transport from the smaller ones), progressively larger particles make up the arrays at increasingly higher temperatures. Methods devised to determine the average particle size, which have been described in considerable detail,[34−36] suggest that ripening of smaller particles results in average particle diameters that increase from ~20 nm at 120 K to ~50 nm at 145 K. Because of the small size, together with adsorbate access from all directions, the diffusion distances of adsorbate molecules required for complete conversion of nanocrystals into a new phase of matter are relatively short. As a result, despite the small values of D_e within hydrate crusts, kinetic measurements throughout the complete conversion process are feasible in the 110−150 K range. By contrast, work with ice films has been largely limited to either ultrathin deposits or to early stages in the conversion of an ice film to a hydrate.

Previous studies have shown that dilute (<20% of monolayer) coverage of ice films[37] or ice nanocrystals[38,39] with HX molecules at temperatures below ~90 K result in a "molecularly" adsorbed state. A matching of FTIR and computed spectra suggests that the adsorbed HX molecules prefer two configurations that differ in their coordination with the surface and/or neighbor-HX molecules: slightly distorted HX molecules with single coordination to surface dangling-oxygen sites and severely distorted doubly coordinated HX, i.e., to surface dangling hydrogen or to a second HX molecule (together with binding to a dangling oxygen). By contrast, even at temperatures as low as 60 K, a full monolayer HX coverage results in rapid formation of a surface layer rich in ionically dissociated HX[11] (proof of a very low activation energy for the basic reaction of adsorbed HX with ice). Self-solvation, leading to 3-coordinated HX molecules, seems to promote this low energy dissociation.[38,40] However, studies have consistently indicated that the ions do not proceed to dissolve in ice. Rather, an increased HX(g) dosage at higher temperatures is required to provide multilayer-adsorbed HX molecules with sufficient free energy to nucleate a new three-dimensional hydrate phase, which may then grow upon additional steady supply of acid.[8,11] Consistent with this view, exposure of an ice array to the saturation pressure of HCl(g) at ~120 K was shown to convert ice nanocrystals to amorphous monohydrate particles over a period of a few hours.[11] More recently, kinetic parameters, from a shrinking-core analysis of FTIR data obtained in the 110−135 K range, were reported for conversions of ice nanoparticles to HCl hydrates.[27] Transitions between hydrates of different acid:water ratios were also observed.

The molecular mechanisms associated with hydrate chemistry are poorly understood; our objective is to generate an experimental database which can be used eventually to advance such understanding. (For the initial efforts toward theoretical analysis, see ref 31.) Experimental evidence indicates collective molecular processes of considerable complexity. For example, past investigation of ice nanocrystal conversion was carried out under conditions of relatively low HCl(g) pressure. After initial nucleation of an amorphous surface phase, with a spectrum resembling an amorphous dihydrate,[38] nucleated 3-D phases displayed spectra corresponding to a much lower acid:water ratio of ~1:6.[27] Eventually, the growth of the increasingly thick amorphous hexahydrate layer slowed due to lengthening of the distance/time scale for acid arrival at the acid-hydrate interface with the ice core. A trihydrate phase was then nucleated at the particle outer surface. Because of an increase in acid diffusion rate with increasing acid:water ratio, the entire hydrate crust then quickly converted to the trihydrate, prior to continuation of reaction with the ice core.

In the present study, conversion kinetics are pursued under significantly higher HX pressures. A hydrate of a high acid-to-water ratio is then nucleated near the beginning of the process and proceeds to grow at constant composition. Moreover, the high acid supply ensures that HX arrival to the surface is not the rate determining step. Rather, slow-down of the ice conversion with time indicates acid diffusion through the product crust as the rate-determining step, enabling determination of the pertinent diffusion coefficient.

Interestingly, hydrate formation (during which all the ice hydrogen bonds are eliminated) is apparently associated with a lower activation energy than the hydrate crystallization, as ice particle reaction with HX below 125 K produces nanoparticles of the amorphous acid hydrates. Amorphous monohydrates crystallize at temperatures above 130 K. Subsequent warming to ~150 K induces rapid desorption of HX into vacuum, transforming the crystalline monohydrate array to the crystalline dihydrate phase. The kinetics can then be examined for the conversion of the crystalline dihydrate to the crystalline monohydrate particles over the range from ~140−155 K under the equilibrium HX (g) vapor pressure.[31] In fact, the kinetic data can be obtained repetitively for a single array by cycling indefinitely between the two crystalline hydrate phases (see Figure 1). (Though not considered in this article, similar cycling between arrays of the crystalline dihydrate and trihydrate is also observed at ~170 K.) For an abundance of HX(g), as provided by the saturation pressure, the rate of the dihydrate to monohydrate conversion is controlled by diffusion of HX through the shell of monohydrate that forms on the particles of the array (vide infra). So, as for the ice-to-hydrate conversions, the shrinking-core model can be used to determine D_e and the HX diffusion activation energy of the crystalline monohydrate.

The cyclic interconversions of the mono- and dihydrate HX crystal phases also make accessible the rate data for the reverse reaction: namely, the mono- to dihydrate conversion through desorption of HX from particle surfaces. This possibility and other identifiable stages of HX interaction/reaction with a 3-D array of ice nanoparticles are summarized in Figure 1. One purpose of this figure is to highlight the existence of a reaction

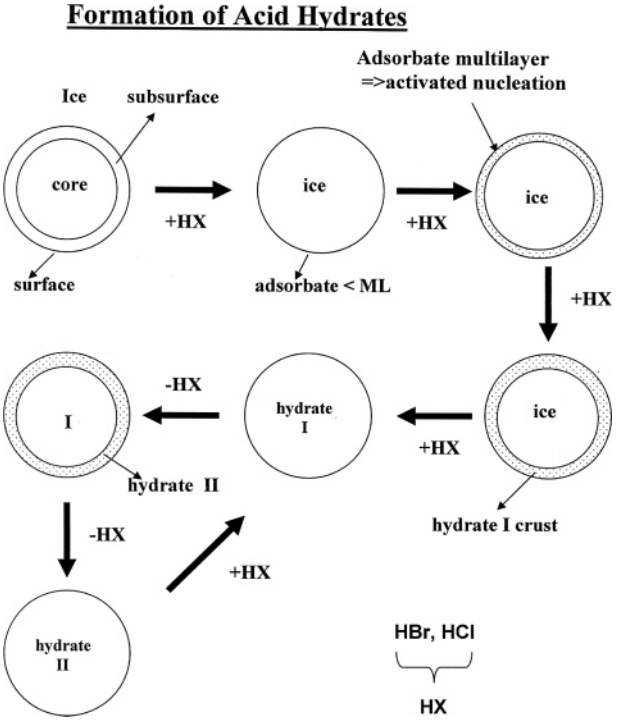

Figure 1. Schematic of the structure of ice nanocrystals indicating multiple levels of uptake of HX acids leading ultimately to acid hydrates. The latter may subsequently interconvert through the gain or loss of HX. Kinetic parameters for ice conversion to a hydrate and for the interconversion of hydrates are the focus of this article.

zone at the interface of the initial and the growing phase with the reaction fed by diffusion of HX molecules, in or out of the particles, through the crust of the growing phase. In this article the focus will be on the rate data for conversion of ice to an amorphous hydrate, and for the two reactions connecting the crystalline dihydrate and monohydrate in the infinite cycle. After examining details of the experiment in section 2, we will first examine the reaction kinetics for HBr (section 3), which are somewhat more straightforward than for HCl. Although some of the details of HCl ice-particle reaction data have been previously published,[27] we will also look briefly at new results for HCl hydrates, with emphasis on the cyclic interconversion of the crystalline mono and dihydrates. The results and analyses of section 3 will be discussed in some detail in section 4, with a summary given in section 5.

2. Experimental Methods

The methods for forming a 3-D array of ice nanocrystals[11,32] and determination of the average particle size[34,42] have been described previously. To enhance the probability that solid-state diffusion of HX molecules controls the rates of hydrate formation and interconversions, dosing was designed to provide an abundance of acid at the surfaces of the particles of the array. This was achieved by simply loading an excessive amount of HX(g) into the cluster cell and making kinetic measurements in the 110−160 K range in the presence of the saturation vapor pressure. Above 110 K, the HX saturation pressures are sufficient to provide continuous (multilayer) coating of the particle surfaces, thereby ensuring that availability of HX at the surface is generally not a rate-limiting factor. The saturation pressures range up from 112 K from the respective HBr and HCl values of ∼1 Pa (0.01 Torr) and ∼50 Pa (0.4 Torr). Differences in temperature of various surfaces within the cluster cell were minimal, since the HX(g) acted as an efficient energy transfer agent.

The identity of the reaction products and the extent of particle conversion to a new phase were both determined using transmission FTIR spectroscopy. The hydrates examined in this study each have well-known infrared spectra that provide a choice of bands for monitoring the extent of reaction.[2,38] However, the quantitative measurement of the amount of ice transformed to hydrate was determined by evaluating the fraction of converted ice through comparison of the sample spectrum with the initial spectrum of the bare nanoparticles. The cyclic interconversion of the monohydrate and dihydrate nanocrystals was similarly followed using the increase/decrease of the intense hydronium-ion stretch band of the monohydrate near 2550 cm^{-1}. In general, prior to reaction, the sample particles were annealed at a temperature sufficiently high that changes in particle size from Ostwald ripening during reaction could be ignored. At the same time, the average particle size was limited so that Mie scattering was not a serious problem. Throughout, the ice particles were prepared from degassed distilled water and dosing was with "Monsanto Grade" HX from which any (relatively) noncondensable gas was first removed.

3. Rate Data for Hydrate Formation from Ice and Hydrate Interconversions

In the previous study of the kinetics of conversion of ice nanocrystals to the amorphous HCl monohydrate, in the presence of the HCl saturation pressure for temperatures ranging from 110 to 125 K, application of the shrinking-core model indicated that the particle reaction rate is determined by the diffusion rate of the acid through the monohydrate crust. The analysis revealed values of the diffusion coefficient in the range $5 \times 10^{-19}-3 \times 10^{-16}$ cm^2/s, implying an associated activation energy of 11 kcal/mol. Here, we report results for the extension of this study to the formation and subsequent interconversion of hydrates of HBr, starting with arrays of ice nanocrystals. New results for the interconversion of the crystalline dihydrate and monohydrate of HCl will also be examined. Ultimately, attention will be drawn to some significant differences in the behavior of the two hydrohalic acids.

3.1. HBr Amorphous Dihydrate Formation and Crystal Hydrate Interconversions. The sequence of reactions investigated was patterned after the possibilities outlined in Figure 1, which are largely derived from the studies of the kinetics of the formation of the hydrates of ammonia and HCl.[26,27] The reaction of an abundance of HBr with an array of ice nanocrystals was found to produce an amorphous dihydrate crust but only after a brief initial phase during which higher hydrates form (Figure 2, bottom spectrum). This early phase is anticipated since the initial HX diffusion distance to the interfacial reaction zone is very short; so acid reacts to form the higher hydrate as rapidly as it is supplied to the surface. (It is known, for example, that the first layer or two of ice reacts rapidly even at 60 K.) As a result, the surface HX concentration does not reach the high level required for nucleation of the dihydrate (HBr) or monohydrate (HCl[27]) until the diffusion distance becomes sufficient that HX arrives at the surface more rapidly than it is converted to the higher hydrate at the receding interfacial reaction zone.

After acid buildup at a particle surface prompts the nucleation of a lower hydrate, that hydrate grows and replaces the higher hydrate in the crust of product surrounding the ice core. However, nucleation of the lower hydrate initially implies the creation of a second reaction zone, as some transport of HX to

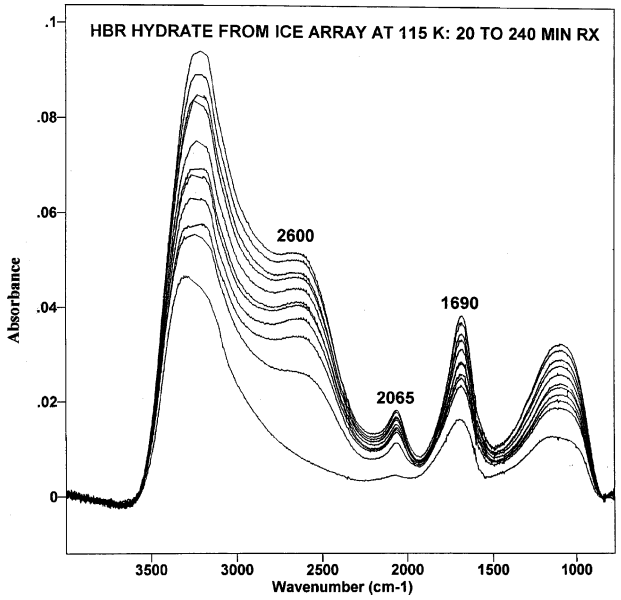

Figure 2. FTIR absorbance spectra of amorphous hydrate product from uptake of HBr from the saturated vapor by ice nanoparticles at 115 K. Note the rapid formation of a higher hydrate during the first 20 min and the subsequent nucleation and growth of the amorphous dihydrate of HBr. The elapsed time from bottom up was, in minutes, 20, 30, 40, 52, 64, 76, 92, 122, 152, 182, and 240.

the original ice-hydrate zone may continue at the same time that the original hydrate converts to the lower hydrate at the new hydrate-hydrate interfacial zone. That a lower hydrate in contact with a higher hydrate is a natural source of HX molecules that diffuse through the higher hydrate will be shown in section 3.1.3. However, provided HX diffusion through the lower hydrate significantly exceeds that through the higher hydrate, the second zone will quickly overtake and eliminate the initial zone; otherwise, two zones can exist throughout much of the ice-particle conversion and the product spectrum will vary with time as the relative amount of the two hydrates in the product crust is altered.

The possible existence of two (or more) reaction zones is not a usual characteristic of particle reactions but results from the stability of as many as five HX (crystalline) hydrates.[43−46] The spectra of Figure 2 strongly suggest that HBr transfer through the dihydrate crust is sufficiently rapid that, once nucleated, the entire crust surrounding the ice core quickly assumes that hydrate phase. From that point, diffusion within the amorphous dihydrate outer-crust can be evaluated using the shrinking core model. The essence of that model can be summarized as follows: the model is based on Fick's 2nd Law (of non-steady state diffusion) as it assumes that the rate of particle conversion is diffusion controlled; which normally requires a constant high surface concentration of adsorbate reactant together with a relatively high rate of interfacial reaction. Rapid interfacial reaction and high nucleation rates, when combined with a high external surface concentration of HX, make the model applicable to the kinetics of acid-hydrate formation within an array of particles.[27]

3.1.1. Formation Kinetics of the Amorphous Dihydrate of HBr. The spectra of Figure 2, of amorphous HBr hydrate forming from an array of ∼25 nm cubic ice crystals at 115 K, show clearly that for the first 20 min of reaction the product is amorphous trihydrate, as reported for HCl reaction with thin layers of ice on a metal substrate.[8] However, the spectrum quickly converts to that of the amorphous dihydrate which shows no further significant variation after 40 min of reaction (3rd scan in the sequence). The dihydrate is recognized from comparison with the published amorphous HX spectra[2] and is best characterized by the pronounced shoulder at 2600 cm^{-1} and the relatively sharp weak feature at 2065 cm^{-1}. A very similar sequence of spectra have also been obtained for the ice particle reaction at 120 and 123 K but the dominance of the dihydrate product spectrum for the higher temperatures comes after only ∼4 and ∼1 min, respectively.

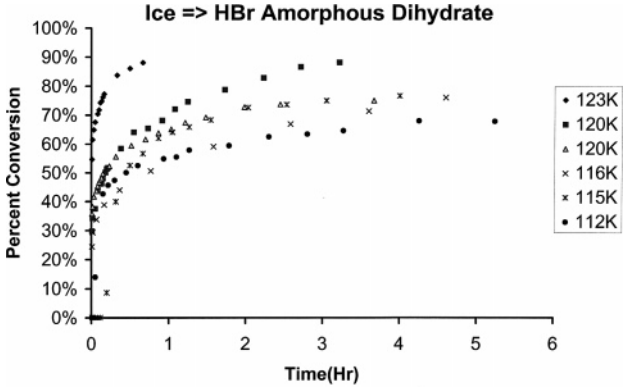

Figure 3. Plot of the percent of ice converted to the amorphous dihydrate of HBr for six (of a total of nine) kinetic runs in the temperature range 112 to 123 K. Though not shown, the plots become linear when the abscissa is time to the power of ∼1/4.

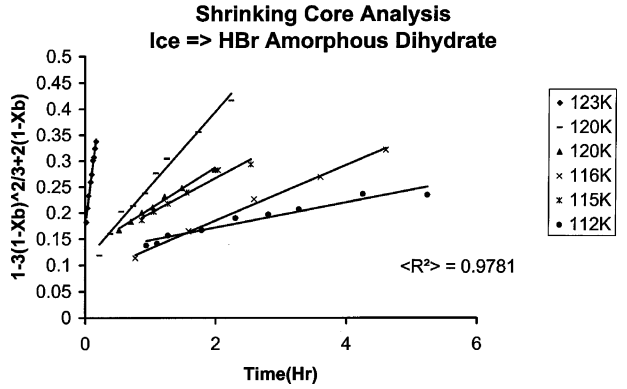

Figure 4. The data of Figure 3 recast as shrinking-core plots as described in refs 28 and 29. The linearity is a sign of rate control by diffusion through the product (hydrate) phase.

The rate data for the conversion of ice particles to the HBr amorphous hydrate are presented in Figure 3. Data points for greater than 88% ice conversion to hydrate are omitted in recognition of the "log-normal" range of particle size; i.e., in addition to the effect of increasing diffusion distance to the interfacial reaction zone, the apparent rate will also eventually slow because of premature complete reaction of the smaller particles.

In Figure 4, each of the data plots of Figure 3, is cast into the form of a shrinking-core-model plot, where X_b is the fraction of reacted ice. The slope, of each of the resulting best-fit straight lines indicated in the figure, can be equated to the set of parameters $6bD_eC_a/R^2\rho$. If each of the parameters, R (particle radius), ρ (particle molar density), b (stoichiometric ratio − HX to H_2O), and C_A (adsorbate, HX, concentration at the particle surface), is known, a diffusion coefficient of HX for the dihydrate can be evaluated from each plot of Figure 4. The ρ and C_A values were approximated as the crystal and liquid-phase values, respectively. The resulting D_e values for HBr in the HBr amorphous dihydrate, for temperatures ranging from 112 to 123 K, are given in Table 1. The corresponding Arrhenius plot of Figure 5 yields an E_a value of ∼7.8 kcal/mol.

TABLE 1: Parameters Determined from Shrinking Core Analysis of HX Hydrate Formation and from Linear Desorption in the Acid-Hydrate Systems

medium	D_e (cm^2/s)	temp. (K)	E_a (kcal/mol)
amorphous $2H_2O{\cdot}HBr$	1.4×10^{-17}	112	7.8
~ 30 nm particles	3.9×10^{-17}	115	
	5.5×10^{-17}	116	
	9.2×10^{-17}	120a	
	8.0×10^{-16}	123	
crystalline $H_2O{\cdot}HBr$	1.4×10^{-17}	146	11.5
~ 50 nm particles	7.7×10^{-17}	150	
	1.1×10^{-16}	152	
	1.1×10^{-16}	156	
	6.8×10^{-16}	160a	
amorphous $H_2O{\cdot}HCl$	4.5×10^{-19}	110	11
~ 30 nm particles[b]	2.8×10^{-18}	115	
	1.0×10^{-17}	120	
	2.8×10^{-16}	125	
$2H_2O{\cdot}HBr$[c] (desorption)		150-160	8.8
$2H_2O{\cdot}HCl$[c] (desorption)		140-152	10.2

[a] Average of two values. [b] From ref 27. [c] Crystalline phase (outer crust).

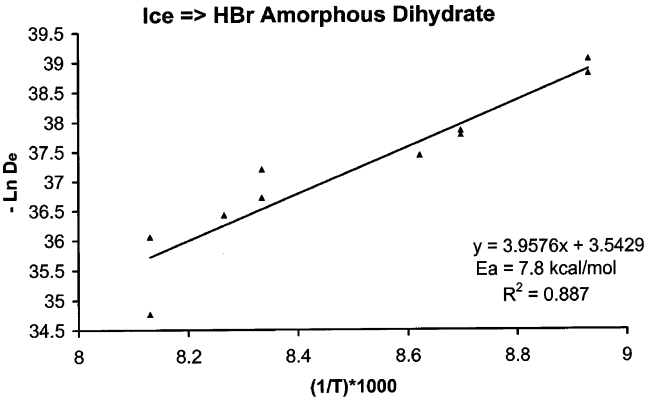

Figure 5. Arrhenius plot and E_a value for the temperature dependence of the diffusion coefficient of HBr in the amorphous dihydrate; from the slopes of the shrinking-core plots for nine samples, as in Figure 4.

3.1.2. Kinetics of Conversion of HBr Crystalline Dihydrate to Crystalline Monohydrate Particles. The amorphous dihydrate of HBr, as formed in the reaction sequence of Figure 2, is kinetically stabilized in a vacuum up to ~140 K, above which temperature it converts to the crystalline dihydrate. If, on the other hand, the HBr saturation pressure is retained to temperatures above ~125 K, the amorphous dihydrate particle array takes up additional HBr while converting to the crystalline monohydrate on a multihour time scale. Subsequent warming of crystalline monohydrate, in a vacuum, at temperatures in the 140−160 K range causes desorption of HBr and slow conversion of the monohydrate particles to the crystalline dihydrate. As noted in Figure 1, this sets up the possibility of an indefinite number of cyclic interconversions of the crystalline forms of the dihydrate and monohydrate of HX through alternating dose and pump stages.

Spectra for the "forward" reaction, of formation of the monohydrate from ~50 nm crystalline dihydrate particles at 160 K by absorption of HBr from the saturated vapor, are presented in Figure 6. There are two striking aspects to the spectra: despite the hour time scale for complete reaction, over 30% of the dihyrate is converted to monohydrate in the first 2 min, and there is a sharply defined isosbestic point near 3000 cm^{-1}. The first aspect is typical of diffusion controlled reactions of

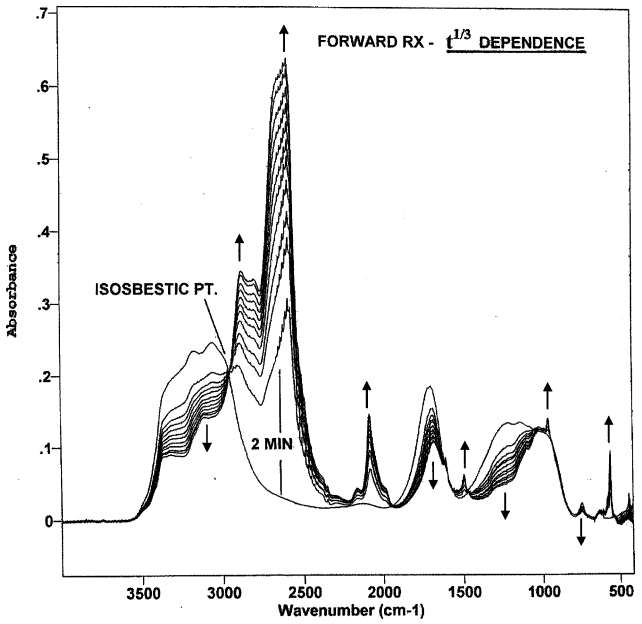

Figure 6. FTIR absorbance spectra for the conversion of the crystalline dihydrate of HBr (down arrows) to the crystalline monohydrate (up arrows) by acid uptake at l60 K from the saturated vapor. Growth of the strong monohydrate band near 2600 cm^{-1} most clearly reflects the extent of conversion at each time.

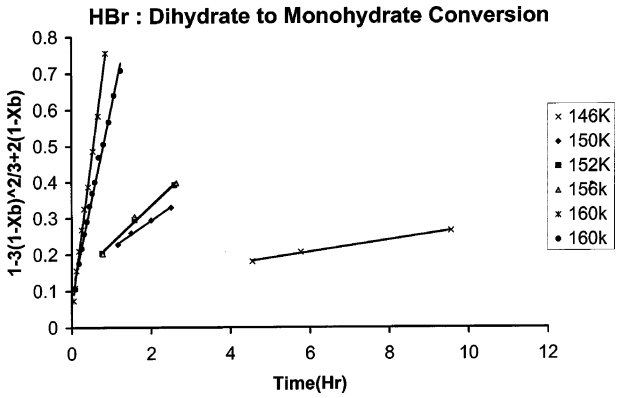

Figure 7. Shrinking-core plots of the rate data for the conversion of crystalline HBr dihydrate to crystalline monohydrate for temperatures ranging from 146 to 160 K.

nanoparticles since significant rapid reaction reflects the short diffusion distances for conversion of the surface region of the particles (see, also, Figure 2). The isosbestic point is important as it demonstrates that there is a narrow sharply defined interfacial reaction zone with no 3rd "phase" that contributes to the O−H stretch region of the spectra. Further, although the HBr must move through the monohydrate crust to reach the monohydrate−dihydrate interfacial zone, it does so without serious impact on the crystal spectra/structure. (In Section 4 we will note properties of the lower acid hydrates that are consistent with this observation.)

Shrinking-core plots of the rate data for six conversions of the crystalline dihydrate to the crystalline monohydrate of HBr are given in Figure 7. The plots are from three repetitive cycles for each of two samples. The linear nature of the individual plots strongly suggests that the rate of di- to monohydrate conversion is determined by diffusion through the monohydrate crust. On that basis, the D_e values from these plots (Table 1) are used in Figure 8 to deduce an Arrhenius activation energy of 11.5 kcal/mol for HBr diffusion in the crystalline monohy-

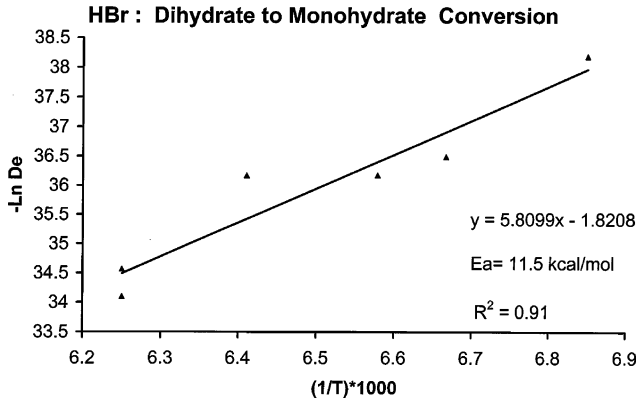

Figure 8. Arrhenius plot and the E_a value from the temperature dependence of the diffusion coefficient of HBr in the crystalline monohydrate crust, using the slopes of the plots of Figure 7.

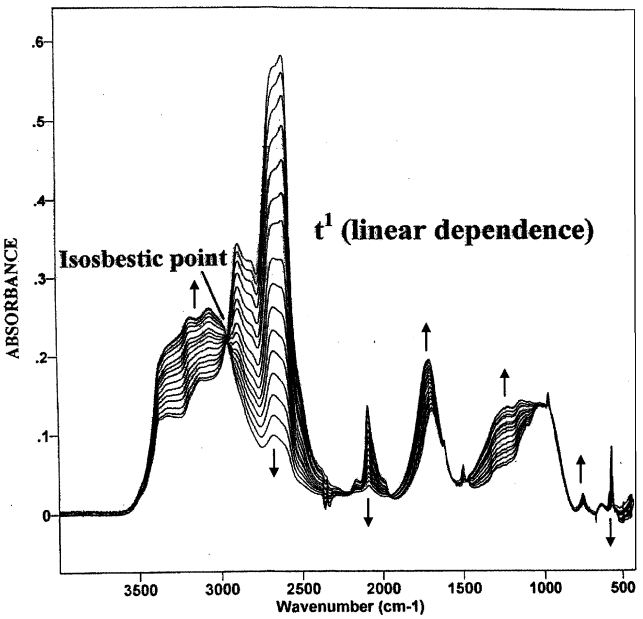

Figure 9. FTIR absorbance spectra for the conversion of crystalline monohydrate of HBr (down arrows) to the crystalline dihydrate (up arrows) through loss of HBr to vacuum. Note the "constant" magnitude of the decrease of the 2600 cm^{-1} monohydrate band for each time step of 14 min.

drate, significantly greater than the 7.8 kcal noted for the amorphous dihydrate in the previous section but consistent with the ~35 K higher temperatures required to give comparable reactions rates.

3.1.3. Kinetics of Conversion of HBr Crystalline Monohydrate to Crystalline Dihydrate Particles: HBr Desorption. An example of the spectra obtained for the reverse process, conversion of the monohydrate to dihydrate, is presented in Figure 9. This series of spectra reflect the loss by desorption of HBr from the dihydrate surface into a moderate vacuum (~10^{-7} bar) at 160 K over a 3 h time period. The spectra were (mostly) obtained with a 14 min time lag between scans. Again, as with the forward reaction to crystalline monohydrate, sharp isosbestic points, such as the one near 3000 cm^{-1}, are indicative of a narrow reaction zone at the interface of the mono and dihydrates. However, in distinct contrast to the forward reaction, it is clear from the spectra that the fractional loss of monohydrate with each 14 min time step is nearly constant throughout most of the conversion to dihydrate. The three data plots of Figure 10 show this linearity and that the rate (slope) is unchanged for

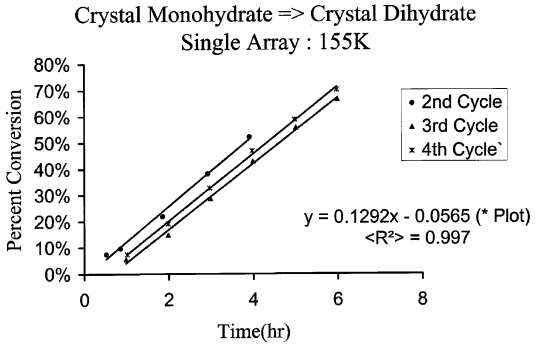

Figure 10. Linear plots vs time of monohydrate to dihydrate crystal conversion through desorption of HBr to vacuum. Note the constant slope for successive uptake-desorption cycles for the same sample at 155 K.

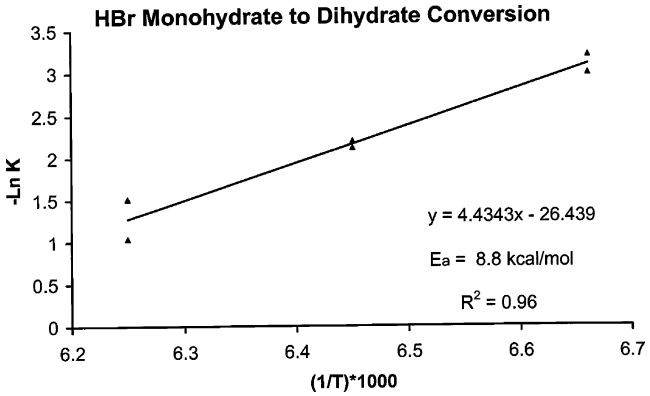

Figure 11. Arrhenius plot and Ea value from the temperature dependence of the desorption rate for the HBr monohydrate to dihydrate conversion from data such as in Figure 10.

the mono-to-dihydrate conversion stage of three successive uptake/desorption cycles at 155 K.

The linear dependence on time of the percent conversion is conclusive evidence that the rate of loss of acid is not determined by HBr diffusion through the increasingly thick dihydrate crust. Rather, the rate is determined by some "constant" of the system. Since the interfacial reaction zone shrinks markedly with time, surface desorption of HBr, rather than release of HBr at the reaction zone, is identified as the rate controlling process. The desorption rate depends on temperature and desorption activation energy, along with the effective area of the particle surfaces. Of these factors, only the surface area is expected to vary during reaction. Based on an estimated ~34% decrease in particle volume[43,46] for complete conversion, the surface area is relatively constant compared to the other possible control factors. (One can note from Figure 9, that beyond ~70% conversion to dihydrate the desorption rate does decrease noticeably; a reduction attributed to a range of particle size, the decrease in interfacial area with conversion, and perhaps the emergence of some dependence on diffusion rate as the reaction zone recedes.)

Data such as that of Figure 10, obtained from 150 to 160 K, are summarized in the Arrhenius plot of Figure 11 and indicate a desorption activation energy of 8.8 kcal/mol for HBr leaving the dihydrate surface. This value can be compared with the somewhat greater value 10.2 kcal/mol for HCl (section 3.2.2).

3.2. HCl Amorphous Hydrate Formation and Crystal−Hydrate Interconversions. The kinetics of the conversion of ice nanocrystals to hydrate particles when exposed to the saturation pressure of HCl in the 110−125 K range has been described.[27] Unlike the HBr system, the HCl−ice product for this temperature range favored the amorphous monohydrate,

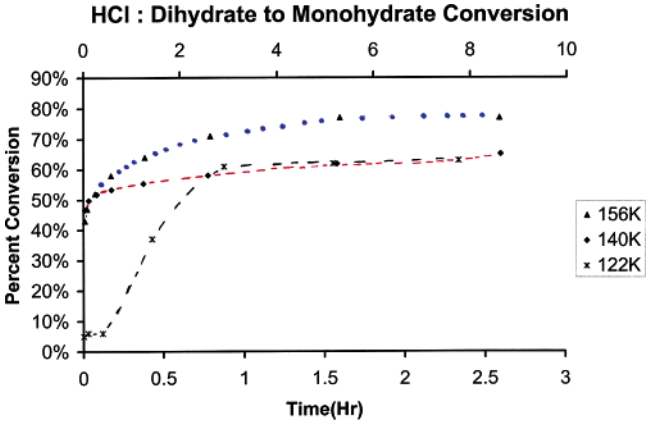

Figure 12. Rate plots for the conversion of the HCl crystalline dihydrate to crystalline monohydrate for temperatures ranging from 122 to 156 K through uptake of the saturated vapor. Note that ~50% conversion occurs within the first minute for the higher temperatures, followed by a rapid falloff in rate. The top time scale is compressed and applies only to data from the 122 K measurements. Curved lines are merely to aid vision.

perhaps at least in part because of the greater HCl saturation pressure. No new quantitative results for this transition are reported here. Rather attention is directed to new rate data for the interconversion of the crystalline mono and dihydrate phases and to the associated D_e and E_a values.

3.2.1. Conversion of HCl Crystalline Dihydrate to Crystalline Monohydrate Particles. Arrays of nanoparticles of the crystalline dihydrate of HCl have been prepared much as described for HBr in section 3.1.2. Once formed, the arrays were exposed to the saturation pressure of HCl in the 140−156 K range. The FTIR spectra obtained during the subsequent conversion to the crystalline monohydrate of HCl possessed the same general characteristics as shown in Figure 6 for the HBr system. Plots of typical data, that reveal the important characteristics of the conversion of crystalline HCl dihydrate to the monohydrate, are given in Figure 12. Most notable are the following: (1) within the temperature range 140 to 156 K, roughly half of the conversion occurs during the first 0.5 min of exposure, and is somewhat more extensive at 140 than 156 K; (2) the initial extremely rapid reaction gives way to a greatly diminished rate, resembling the diffusion control described for the parallel HBr process (section 3.1.2) with the subsequent conversion clearly accelerated at higher temperatures; (3) the ~50% initial conversion occurs at a much slower rate at 122 K, indicating an activated process (despite the greater reaction during the first minute at 140 vs 156 K), with conversion then stopping completely on a laboratory time scale. Since HX reacts rapidly with an ice array at 122 K (Figure 3), the slow initial phase cannot reflect limited access of acid to the dihydrate array.

These curious results will be considered in some detail in Section 4 in light of insights from the defect-based Monte Carlo particle-reaction model. Here it is noted that the reaction pattern of Figure 12, which seems to indicate two overlapping reaction stages with very different rate factors, has not proven to be compatible with a quantitative evaluation of kinetic parameters for the conversion of nanocrystals of the dihydrate to nanocrystals of the monohydrate.

3.2.2. Kinetics of Conversion of HCl Crystalline Monohydrate to Crystalline Dihydrate Particles. In contrast with the formation of the monohydrate, desorption of HCl produces the crystalline dihydrate smoothly and in near perfect parallel with the corresponding HBr reaction. Essentially linear loss of the monohydrate as a function of time is apparent from the four

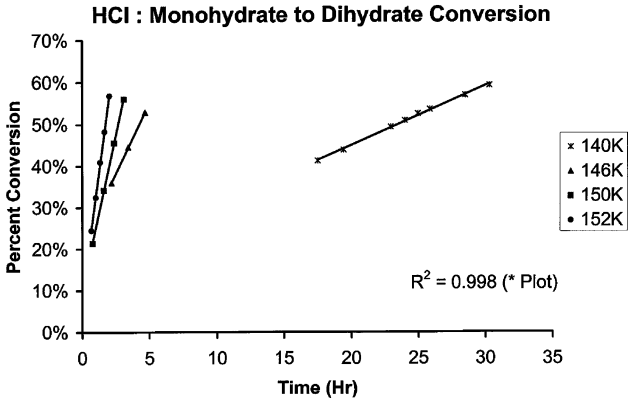

Figure 13. Same as for Figure 9, except for HCl crystalline hydrates, with a temperature range of 140−152 K.

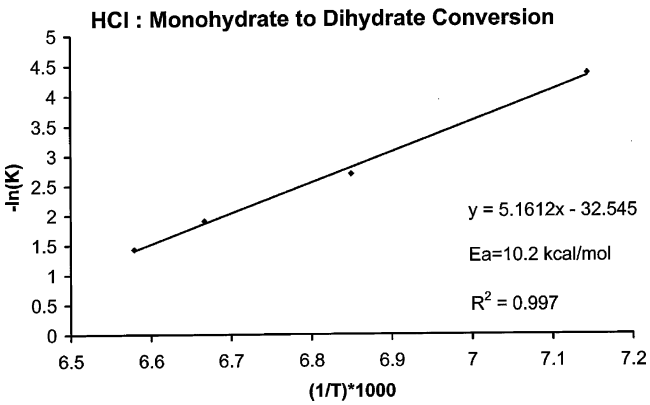

Figure 14. Same as for Figure 11, except for HCl.

plots of Figure 13. However, extension of the conversion to >60% would show a gradual decrease in rate slightly more pronounced than noted for the HBr systems. The data of Figure 13 lead to the Arrhenius plot of Figure 14 and the value 10.2 kcal·mol for HCl desorption from the dihydrate surface. This is significantly greater than the corresponding HBr value of 8.8 kcal/mol of section 3.1.3.

4. Discussion

In general the analysis of the experimental data, for the conversion of ice particles to acid hydrate particles and the interconversion of HX hydrate particles, suggests that the forward reactions, with uptake of HX, proceed with a rate determined by the diffusion of the acid through the outer crust of hydrate provided there is an abundance of adsorbed HX on the outer particle surface. This is consistent with earlier results reported for ice particle reaction with ammonia and HCl,[27] as well as HBr crystal dihydrate conversion to the crystal monohydrate.[31] By contrast, the new data for desorption of HX from crystal hydrate particles, during formation of the next higher hydrate, point to near constant conversion rates apparently determined by desorption rates of HX from the surface of a crust of the higher hydrate. Quantitative results for the various systems are summarized in Table 1 with specific aspects and implications of the results considered below.

4.1. Uptake of HX by Ice and Crystalline Dihydrates. A number of questions can be raised that relate to the extensive uptake of HX by particles to form acid hydrates from ice, or to convert a higher to a lower hydrate. These include: (1) the role of diffusion of acid in ice, (2) the applicability of the shrinking-core model to the kinetic data, i.e., the rate controlling processes,

(3) the molecular/ionic nature of acid transport to the reaction zone, (4) the magnitudes of the diffusion coefficients for the transport processes (Table 1: D_e), and (5) the values of the diffusion activation energies (Table 1: E_a) and (6) the identity of molecular factors that determine the D_e and E_a values.

An evaluation of the role of diffusion in ice is related to the applicability to the kinetic data of the shrinking-core model of particle reaction. Straight-line plots based on that model, such as presented in Figures 4 and 7, offer strong support for the concept of interfacial reaction zones, with the conversion rate determined by the diffusion of HX through the crust of the hydrate product to the interface with the reacting core.[28,29] There can be little doubt that this description applies to the conversion of crystalline HBr dihydrate to monohydrate, since the sharp isosbestic points of Figure 6 offer clear evidence of a narrow interfacial zone. Similarly, the spectra at most stages of the conversion of ice particles to the amorphous HBr dihydrate can be closely fit using the spectrum of the ice and the dihydrate spectra of Figure 2. For this view of the conversion process, there is no need to invoke diffusion in the ice (core) of the particle. In any case, the quantity of HX that diffuses into ice has been shown to be extremely limited by a natural low solubility in ice.[25]

The configuration of an array of particles undergoing conversion to a new phase through reaction with HX adsorbate suggests that the factors which might influence the conversion rate include the surface nucleation rate of the new phase, the surface density of adsorbate (HX), total particle external surface area, the reaction rate and area at the interfacial zone, and the diffusion rate of HX to that reaction zone. Two of these processes are extremely rapid and, therefore, cannot be rate limiting: namely the basic reaction rate, which is fast even at 60 K, and the nucleation rate which must be rapid to give the exceptionally high initial reaction rates evidenced in Figures 3 and 6. Two other candidates, namely, the surface density of adsorbate molecules and the total surface area are roughly constant throughout these conversions; so cannot be the source of a $\sim t^{1/4}$ dependence observed for the fractional conversion of the reactant particles.[31] This leaves the single factor of diffusion rates of HX to the reaction zone, values of which are revealed (in the shrinking-core analysis) as rate controlling.

The mechanism and form by which HX diffuses through the product crust to the reaction zone is not known but qualitative suppositions can be offered. In particular, the question arises as to whether the HX diffuses as a molecular or ionic entity. It has been shown conclusively that the diffusion of NH_3 to the reaction zone during formation of its hemihydrate from ice particles is strictly molecular, since no isotopic exchange occurs in the formation of $2NH_3 \cdot D_2O$.[26] By contrast, the ionic HX hydrates apparently form with complete isotopic scrambling. For example, the monohydrate can be largely converted to the monodeuterate by exposure to DCl(g) for several hours at 155 K. However, there is spectroscopic evidence of a significant molecular population of HX within most of the primarily ionic amorphous and crystalline hydrates. On the basis of ab initio calculations for models of water-HCl clusters,[38] and in the absence of any alternate assignment, the relatively narrow band at 2065 cm^{-1} in the amorphous HBr dihydrate spectrum (Figure 2), which also appears in the same frequency region for the amorphous and crystalline tri-, di-, and monohydrates of both HCl and HBr (Figures 2 and 6 and ref 2), has been assigned to interstitial molecular HX attached to halide ions of the solid structures. Consistent with that assignment, these bands are strongest for the most acid-rich structures, namely the amorphous and crystalline monohydrate, and are probably not detectable in the hexahydrate spectra.

Given the higher population of HX molecules in the lower hydrates, the evidence that HX diffusion to the reaction zone is much more rapid in the lower than the higher hydrates[27] is consistent with a molecular diffusion mechanism for the hydrate series. Also favoring this "molecular" view is the seeming improbability of rapid diffusion of tightly bound halide ions through the hydrate structures at temperatures as low as 120 K.

The concept of HX transport can be further developed using the results of our recent Monte Carlo (MC) model, which provides a description of the stages of conversion of a pure particle of substance A coated with substance B to the mixed phase, AB.[31] In the model, A, B, and AB solids are assumed to be crystalline, with A and B particles distributed on a simple cubic lattice; material transport occurs via vacancy−defect jumps. Growth of the new AB phase was initiated by multisite nucleation at the particle surface. Then, with the defect operating preferentially in the interfacial regions between the phases, motion favorable to transport of reactant molecules to the interfacial reaction zone was generated (Figure 11 of ref 31). The reaction, similar in time dependence to Figures 3 and 6, was advanced by transport of reactants along the interfacial boundaries and generated a "shrinking core" of particle A.

The model is much simpler than the hydrate systems considered here, but some of the conclusions are likely to apply. Let us consider the reaction of HX with the crystal dihydrate to form a monohydrate nanocrystal. One can still reasonably expect the validity of multisite nucleation at the surface, and preferential flow of material along the defective grain boundaries, rather than through the well-crystallized product. The defect species responsible for transport might include a combination of vacancies and molecular HX. One may note in this context that 1:1 and 1:2 clusters of HX with water are molecular; thus, one must envisage ionization in the hydrate environment as being induced by mutual solvation of cluster units arranged in a symmetric pattern. Acid ionization is likely to be less effective in the asymmetric and defective grain-boundary environment, resulting in enhanced population of the more weakly bound and more mobile HX. As noted above, the observed FTIR band of an HX impurity is consistent with molecules attached to X^- ions, perhaps primarily at the grain boundaries. The mobility of HX can be imagined to consist of acid molecules moving from halide to halide sites on the interfacial "surfaces". Not all such sites will be populated with HX and the motion of vacant sites would be analogous to the motion of a vacancy defect, with associated transport of HX. However, in contrast to the MC model, the crystal structures of the mono- and dihydrate are different from each other; and a grain boundary between two different crystals is likely to be an even more effective conduit for material flow than a boundary between two grains of the same material (moreover, the former constitutes the reaction zone). Perhaps the experimentally observed extreme initial efficiency of the reaction is associated with the flow of HX around individual nucleated grains, at the boundary between the mono- and the dihydrate; while the subsequent slow-down is associated with formation of a "continuous" crust of crystal monohydrate around the dihydrate core. The latter rate slows further as the particle core recedes and the path of HX to the reaction zone lengthens (i.e., to the mono- and dihydrate interface); e.g., see Figures 3 and 6 and Figure 11 of ref 31.

The unexpected result for the conversion of HCl dihydrate to monohydrate particles (Figure 12), with ~50% conversion

occurring in the first minute of a process that ultimately proceeds for hours, requires additional consideration. Since the particles of an array must be severely flexed by growth/shrinkage during the conversion from one phase to another, it is likely that fissures are produced particularly in the outer regions of the particles. These fissures, incompletely healed at the low reaction temperatures (~140 K), may then constitute additional interfacial regions, which, like those produced by multiple nucleation sites, accelerate the movement of HCl to reaction zones within a particle. Perhaps, after reaction of the outer reaches of a particle, such fissures would no longer participate, causing the rate to rapidly decay to one more familiar from simpler diffusion controlled processes such as that of Figure 3. This effect is apparently more important for the HCl than the HBr system.

The grain boundary mechanism may or may not apply to material flow in the amorphous hydrate, the rate-determining process in the lower temperature ice-conversion experiments. As argued above, the amorphous hydrate is a nucleated phase; however different nucleated amorphous grains might merge more smoothly into each other than the crystal ones discussed above. On the other hand, an amorphous material is naturally defect-rich, and defect jumps promote material transport. One may note in this context a recent computational study of amorphous H_2O which demonstrated that (i) structural defects (in that case 3- and 5-coordinated H_2O) are mobile at remarkably low temperatures and (ii) during a defect jump neighboring molecular material is reshuffled; thus, defect jumps are associated with material transport[47] (these results are consistent with experimentally observed orientational and translational mobility in amorphous H_2O.[41,48] According to spectroscopic evidence,[38] amorphous monohydrate includes H_3O^+, $H_5O_2^+$, and X^- ions, together with some molecular HX bonded to the halide. The simplest diffusion mechanism would correspond to HX-impurity diffusion through the hydrate, by bond switching from one halide ion to another. A more complex process would involve interconversion between the different components (such as proton transfer between the HX and the halide, or water transfer from Zundel to hydronium ions), with concurrent local reshuffling of the surrounding molecular material.

It is interesting to note that acid mobility within the amorphous monohydrate is higher than within the crystal, once the fast initial phase of the crystal reaction is completed (and presumably, a continuous crust of crystal monohydrate is formed around the dihydrate core). This finding is evident from comparison of the pertinent 122 K results: ice nanoparticle conversion to amorphous HCl monohydrate proceeds to completion,[27] while conversion of crystal HCl dihydrate to monohydrate virtually stops after the initial fast phase (see Figure 12).

The physical basis of the diffusional activation-energy values of Table 1 is of interest. This energy is likely to be associated with the energy to detach an HX molecule from binding with a halide ion so that the HX moves to the next site. The absolute value of this binding energy is not known for the solid hydrates, but one can argue that it should be lower for HBr than for HCl as is the case for E_a in Table 1 (i.e., 7.8 vs 11 kcal/mol). The frequency of the HBr stretch, of bromide-bound HBr of Figure 2 (2065 cm^{-1}), represents a shift of 495 cm^{-1} vs the gas-phase value of 2560 cm^{-1}. By contrast HCl interacting with chloride ion in amorphous HCl monohydrate experiences a ~760 cm^{-1} shift, to 2110 cm^{-1}[2], from the gas-phase value of 2891. The respective shifts, that indicate the halide binding is greater for HCl than HBr, are thus consistent with the conjectured diffusion mechanism presented above.

4.2. HX Desorption: Conversion of HX Crystalline Monohydrates to Dihydrates. It is interesting that desorption rather than diffusion controls the reverse reaction: namely the loss of HX to form a higher hydrate. This rate control has been shown for mono- to dihydrate conversion for both HBr and HCl (section 3.2) and for the di- to trihydrate conversion (as an initial part of a study not considered in detail here). A similar activation energy as the one obtained for diffusion suggests that breaking of the HX bond to the surface halide ion is again involved. The question might arise as to whether desorption will invariably be rate controlling for phase conversions involving molecular loss from H-bonded mixed solids. Clearly, more comparative experimental/computational results are needed.

5. Summary Conclusions

Arrays of ice nanocrystals convert in a matter of hours to the amorphous monohydrate of HCl[27] and dihydrate of HBr, under saturation pressures of the acids at temperatures in the 110−125 K range. Crystalline dihydrate particles of HX convert to the crystalline monohydrates on a similar time scale for temperatures in the 140−155 K range (following an initial fast reaction stage which appears to be associated with boundaries from fragmented coverage of the particle surfaces by the nucleated product). Application of a shrinking-core model to quantitative kinetic data for these phase conversions has identified the rate controlling process as HX diffusion through the product crust. This has enabled the evaluation of D_e and HX diffusion activation energy values for various product phases. A conjecture has been made of the mechanism by which HX molecules diffuse through a crystal hydrate to the interfacial reaction zone. It is proposed that diffusion is primarily molecular, sustained by HX jumps between halide sites along the grain boundaries; the boundaries being a consequence of multisite surface nucleation. The conjecture is supported by the ease with which hydrates interconvert through gain or loss of HX, evidence of the presence of (transiently) molecular HX complexed with halide ions within the hydrates[38] and the relative magnitude of E_a found for HBr and HCl diffusion. HCl, which binds more strongly to the halide ion, has the greater E_a values, and D_e increases from the higher to lower hydrates[27] as does the HX population. Comparison of 122 K data indicates more efficient acid diffusion through the amorphous HCl monohydrate than through the crystal crust. In a defect-rich amorphous phase, material flow through the entire crust volume may be effective.

Rates of conversion of crystalline monohydrate particles to the dihydrate phase, as well as of the dihydrate to the trihydrate, have also been determined. The rates of such phase changes, a result of desorption loss of HX, are not controlled by HX diffusion. Rather, the rate in each case is nearly constant throughout the particle conversion, which identifies desorption of HX from the particle surfaces as rate controlling. As in the case of the activation energies for the uptake of HX, the activation energies for desorption were found to be somewhat greater for HCl than HBr.

Acknowledgment. Support of this research by the National Science Foundation under grant CHE - 0243019 is gratefully acknowledged.

References and Notes

(1) Horn, A. B.; Sodeau, J. R. In *Water in Confining Geometries*; Buch, V., Devlin, J. P., Eds.; Springer: Berlin, 2003; Chapter 13, p 295.

(2) Delzeit, L.; Rowland, B.; Devlin, J. P. *J. Phys. Chem.* **1993**, *97*, 10312.

(3) Barone, S. B.; Zondlo, M. A.; Tolbert, M. A. *J. Phys. Chem. A* **1999**, *103*, 9717.
(4) Isakson, M. J.; Sitz, G. O. *J. Phys. Chem. A* **1999**, *103*, 2044.
(5) Sadtchenko, V.; Giese, C. F.; Gentry, W. R. *J. Phys. Chem. B* **2000**, *104*, 9421.
(6) Hudson, P. K.; Foster, K. L.; Tolbert, M. A.; George, S. M.; Carlo, S. R.; Grassian, V. H. *J. Phys. Chem. A* **2001**, *105*, 694.
(7) Andersson, P. U.; Nagard, M. B.; Pettersson, J. B. C. *J. Phys. Chem. B* **2000**, *104*, 1596.
(8) Haq, S.; Harnett, J.; Hodgson, A. *J. Phys. Chem. B* **2002**, *106*, 3950.
(9) Chu, L. T.; Leu, M. T.; Keyser, L. F. *J. Phys. Chem.* **1993**, *97*, 7779.
(10) Hanson, D. R.; Ravishankara, A. R. *J. Phys. Chem.* **1992**, *96*, 2682.
(11) Delzeit, L.; Powell, K.; Uras, N.; Devlin, J. P. *J. Phys. Chem. B* **1997**, *101*, 2327.
(12) Banham, S. F.; Horn, A. B.; Koch, T. G.; Sodeau, J. R. *Faraday Discuss.* **1995**, *100*, 321.
(13) Banham, S. F.; Sodeau, J. R.; Horn, A. B.; McCoustra, M. R. S.; Chesters, M. A. *J. Vac. Sci. Technol. A* **1996**, *14* (3), 1620.
(14) Schaff, J. E.; Roberts, J. T. *J. Phys. Chem.* **1996**, *100*, 14151.
(15) Blanchard, J. L.; Roberts, J. T. *Langmuir* **1994**, *10*, 3303.
(16) Graham, J. D.; Roberts, J. T. *J. Phys. Chem.* **1994**, *98*, 5974.
(17) Graham, J. D.; Roberts, J. T. *Geophys. Res. Lett.* **1995**, *22*, 251.
(18) Foster, K. L.; Tolbert, M. A.; George, S. M. *J. Phys. Chem. A* **1997**, *101*, 4979.
(19) Livingston, F. E.; George, S. M. *J. Phys. Chem. A* **1998**, *102*, 10280−10288.
(20) Livingston, F. E.; George, S. M. *J. Phys. Chem. A* **2001**, *105*, 5155−5164.
(21) Koehler, B. G.; Middlebrook, A. M.; McNeil, L. S.; Tolbert, M. A. *J. Geophys. Res.* **1993**, *88*, 10563.
(22) Horn, A. B.; Sully, J. *J. Chem. Soc., Faraday Trans.* **1997**, *93*, 2741.
(23) Molina, M. J.; Tso, T. L.; Molina, L. T.; Wang, F. C. Y. *Science* **1987**, *238*, 1253.
(24) Livingston, F. E.; Smith, J. A.; George, S. M. *J. Phys. Chem. A* **2002**, *106*, 6309−6318.
(25) Thibert, E.; Domine, F. *J. Phys. Chem. B* **1997**, *101*, 3554−3565.
(26) Uras, N.; Devlin, J. P. *J. Phys. Chem. A* **2000**, *104*, 5770.
(27) Uras-Aytemiz, N.; Joyce, C.; Devlin, J. P. *J. Phys. Chem. A* **2001**, *105*, 10497.
(28) Carter, R. E. *J. Chem. Phys.* **1960**, *34*, 2010.
(29) Levenspiel, O. *Chemical Reaction Engineering*; Wiley & Sons: New York, 1962.
(30) Wang, X.; Schultz, A. J.; Halpern, Y. *J. Phys. Chem. A* **2002**, *106*, 7304−7309.
(31) Yinnon, C. A.; Buch, V.; Devlin, J. P. *J. Chem. Phys.* **2004**, *120*, 11200−11208.
(32) Devlin, J. P.; Buch, V. *J. Phys. Chem.* **1995**, *99*, 16534.
(33) Buck, U.; Steinbach, C. In *Water in Confining Geometries*; Buch, V., Devlin, J. P., Eds.; Springer: Berlin, 2003; Chapter 3, p 53.
(34) Devlin, J. P.; Sadlej, J.; Buch, V. *J. Phys. Chem. A* **2001**, *105*, 974.
(35) Delzeit, L.; Blake, D. *J. Geophys. Res.—Planets* **2001**, *106* (E12), 33371.
(36) Buch, V.; Bauerecker, S.; Devlin, J. P.; Buck, U.; Kazimirski, J. K. *Int. Rev. Phys. Chem.* **2004**, *23*, 375.
(37) Kang, H.; Shin, T. H.; Park, S. C.; Kim, I. K.; Han, S. J. *J. Am. Chem. Soc.* **2000**, *122*, 9842.
(38) Buch, V.; Sadlej, J.; Uras-Aytemiz, N.; Devlin, J. P. *J. Phys. Chem. A* **2002**, *106*, 9374.
(39) Devlin, J. P.; Uras, N.; Sadlej, J.; Buch, V. *Nature* **2002**, *417*, 269.
(40) Svanberg, M.; Pettersson, J. B. C.; Bolton, K. J. *J. Phys. Chem. A* **2000**, *104*, 5787.
(41) Fisher, M.; Devlin, J. P. *J. Phys. Chem.* **1995**, *99*, 11584.
(42) Devlin, J. P.; Buch, V. In *Water in Confining Geometries*; Buch, V., Devlin, J. P., Eds.; Springer: Berlin, 2003; Chapter 17, p 425.
(43) Lundgren, J. D.; Olovsson, I. *Acta Crystallogr.* **1967**, *23*, 966.
(44) Lundgren, J. D.; Olovsson, I. *Acta Crystallogr.* **1967**, *23*, 971.
(45) Taesler, I.; Lundgren, J. O. *Acta Crystallogr.* **1978**, *B34*, 2424.
(46) Yoon, Y. K.; Carpenter, G. B. *Acta Crystallogr.* **1959**, *12*, 17.
(47) Grishina, N.; Buch, V. *Chem. Phys. Lett.* **2003**, *379*, 418−426.
(48) Smith, R. S.; Dohnlek, Z.; Kimmel, G. A.; Stevenson, K. P.; Kay, B. D. *Chem. Phys.* **2000**, *258*, 291.